Solar Phys (2010) 261: 363–373
DOI 10.1007/s11207-009-9500-0

ROSA: A High-cadence, Synchronized Multi-camera Solar Imaging System

D.B. Jess · M. Mathioudakis · D.J. Christian · F.P. Keenan · R.S.I. Ryans · P.J. Crockett

Received: 2 July 2009 / Accepted: 21 December 2009 / Published online: 13 January 2010
© Springer Science+Business Media B.V. 2010

Abstract The Rapid Oscillations in the Solar Atmosphere (ROSA) instrument is a synchronized, six-camera high-cadence solar imaging instrument developed by Queen's University Belfast. The system is available on the Dunn Solar Telescope at the National Solar Observatory in Sunspot, New Mexico, USA, as a common-user instrument. Consisting of six 1k × 1k Peltier-cooled frame-transfer CCD cameras with very low noise ($0.02-15$ e s^{-1} pixel^{-1}), each ROSA camera is capable of full-chip readout speeds in excess of 30 Hz, or 200 Hz when the CCD is windowed. Combining multiple cameras and fast readout rates, ROSA will accumulate approximately 12 TB of data per 8 hours observing. Following successful commissioning during August 2008, ROSA will allow for multi-wavelength studies of the solar atmosphere at a high temporal resolution.

Keywords Instrumentation and data management

1. Introduction

Performing high-cadence observations of astronomical sources is a growing field within astrophysics, and there is a clear need for such data for the Sun. Many research topics, in particular those related to the dynamic Sun and the heating of its outer regions, involve the observation and modeling of wave phenomena and explosive events captured over very short time scales. High-cadence observations are also important for post-facto image reconstruction (PFIR) techniques, which require the processing of an extensive collection of images for

D.B. Jess (✉) · M. Mathioudakis · F.P. Keenan · R.S.I. Ryans · P.J. Crockett
Astrophysics Research Centre, School of Mathematics and Physics, Queen's University Belfast, Belfast, BT7 1NN, Northern Ireland, UK
e-mail: d.jess@qub.ac.uk

D.J. Christian
Department of Physics and Astronomy, California State University Northridge, 18111 Nordhoff Street, Northridge, CA 91330, USA

the production of a single frame at diffraction-limited resolution. These short exposure images must be accumulated over time scales sufficiently small so that atmospheric turbulence is effectively "frozen out", and the solar features remain unchanged.

Since the discovery of solar oscillations in the 1960s (Leighton, 1960), and their subsequent confirmation by Deubner (1975), there has been a multitude of observational evidence presented verifying the widespread existence of oscillations in the solar atmosphere (see the recent review by Banerjee *et al.*, 2007). Oscillations throughout the solar atmosphere have enabled scientists to probe the underlying physics involved in energy transfer and coronal heating, and have been suggested as candidates to explain one of the main unanswered questions in solar physics: *Why is the outer solar atmosphere hotter than its surface?* However, in recent years the need to probe high-frequency oscillations has arisen. Porter, Klimchuk, and Sturrock (1994) have shown that the energy contribution of high-frequency waves to atmospheric heating may be significant. Furthermore, Hasan and van Ballegooijen (2008) have indicated that quasi-periodic oscillations shorter than 100 s may be a vital mechanism in the creation of the multi-million degree solar corona. Thus, a sensitive camera system with a suitably high cadence to satisfy the Nyquist parameter is paramount for the study of high-frequency oscillations.

Such a system is not only capable of studying wave motion, but may also be utilized to examine highly dynamic phenomena in the lower solar atmosphere. Recently, fast-moving plasma with velocities exceeding 200 $\mathrm{km\,s^{-1}}$ has been observed by van Noort and Rouppe van der Voort (2006), indicating the abundance of highly dynamic structures in the chromosphere. Additional investigations may include the search for hard X-ray non-thermal electron precipitation sites in the event of flare activity. Kiplinger *et al.* (1983) report short duration spikes associated with hard X-ray emission from solar flares, and in conjunction with the impact of fast-moving non-thermal electrons, this leads to enhanced emission over inherently short time scales (< 0.04 s; Brown, 1971). This, coupled with the detection of fast fluctuations of Hα emission from a flare kernel on time scales of $0.3-0.7$ s by Wang *et al.* (2000), demonstrates the need for high-cadence solar imaging techniques to capture these dynamic processes on their intrinsic scales.

The search for rapid, often low-amplitude intensity variations requires a highly sensitive camera system providing accurate, sustained frame rates, accompanied by good local seeing at the telescope facility. Here we report the construction of a new high-speed camera system, developed by Queen's University Belfast (QUB), and its commissioning as a common-user instrument at the Dunn Solar Telescope (DST) facility run by the National Solar Observatory in the Sacramento Peak mountains, New Mexico, USA. This system, named *Rapid Oscillations in the Solar Atmosphere* (ROSA), will present users with the ability to observe the Sun simultaneously in up to six wavelengths or wavebands. A detailed guide to ROSA's hardware is described in Section 2, while in Section 3 a description of available observing modes is presented. In Section 4 ROSA's graphical user interface (GUI) is explained, followed by guidelines for obtaining calibrated data in Section 5. Finally, concluding remarks, in addition to sample images from the instrument commissioning, are given in Section 6.

2. Instrumentation

In the late 1990's, a high-speed, two-camera solar imaging system named the *Solar Eclipse Corona Imaging System* (SECIS; Phillips *et al.*, 2000) began development. This instrument was designed to rapidly capture images of the solar corona during a total eclipse and produced some very interesting results (see *e.g.* Williams *et al.*, 2001, 2002; Katsiyannis *et al.*,

Table 1 Detailed description of ROSA camera characteristics.

Camera Parameter	Specification
Model	Andor iXon+ DU-885K-VP
Pixels	1004×1002
Pixel Size	8×8 μm
Maximum Frame rate (full chip)	$30\ s^{-1}$
Maximum Frame rate (windowed chip)	$200\ s^{-1}$
Read noise	$15\ e\ s^{-1}\ pixel^{-1}$
Data output	14 bit

2003). However, in order to image the lower solar atmosphere at high time resolution, a new camera system needed to be developed. The *Rapid Dual Imager* (RDI; Jess *et al.*, 2007a) was designed as a followup to the highly successful SECIS camera system and consists of two 502×494 pixel^2 CCDs, operating at speeds of up to 20 frames per second. Even with a relatively small number of pixels and onboard storage, RDI was able to show the need for a dedicated high-cadence multi-camera system (see *e.g.* Jess *et al.*, 2007b) and acted as a pre-cursor to the capabilities possessed by ROSA.

The ROSA system consists of six individual frame-transfer CCDs, each with their own dedicated server for data acquisition and storage. All cameras are triggered via a Precision Control Unit or "sync" box. The CCD cameras are from Andor Technologies of Belfast, with the DU-885-VP model chosen comprising of a 1004×1002 pixel^2 area. They are cooled up to 100°C below ambient temperature through use of a thermoelectric Peltier cooler. Maintaining low readout noise necessary for fast readout rates, each ROSA camera can read out over 30 frames per second in full-chip mode and over 200 frames per second when the CCD is windowed. The CCD characteristics specific to the ROSA system are presented in Table 1 and further described in Section 2.1.

The sync box provides independent 5 V DC pulses to each of the ROSA cameras to control the frame acquisition at preset trigger rates. Four trigger rates can be specified by the telescope user based upon the filters and exposure times chosen. As a result, all six cameras can be triggered at the same synchronized frame rate, or by any combination of the user-defined trigger rates. The sync box receives information from the master computer through a USB connection and is hard-wired to each ROSA camera via individual 5 m cables. Timing errors related to the arrival of synchronous pulses from different trigger cables are < 30 μs.

Each camera has its own dedicated high-speed server that controls the data acquisition and storage. The PCs are Dell PowerEdge 2900 dual-core Xeon units, each with 4 GB RAM and over 1 TB of onboard storage. To achieve sustained frame rates and prevent data corruption, each ROSA server consists of eight high-speed (15 000 RPM) hard drives, running in a RAID 0 configuration to boost available storage. All six servers are mounted in two, wheeled-rack enclosures, allowing the entire system to be re-positioned easily. Control of the six independent PCs can be achieved through use of a master server (also stored within the rack-mounted enclosure), where a KVM module allows each individual computer's display to be piped to a single screen.

Running at a sustained frame rate of 30 frames per second in all six ROSA cameras, approximately 1.3 TB of data are accumulated every hour. The data are written into a flexible image transport system (FITS; Hanisch *et al.*, 2001) format, incorporating a header and multiple image extensions. Detailed information related to the observing sequence is written in the main FITS header and includes descriptions of both the CCD and observing parameters, in addition to the acquisition start time. Each FITS file contains 256 individual images to

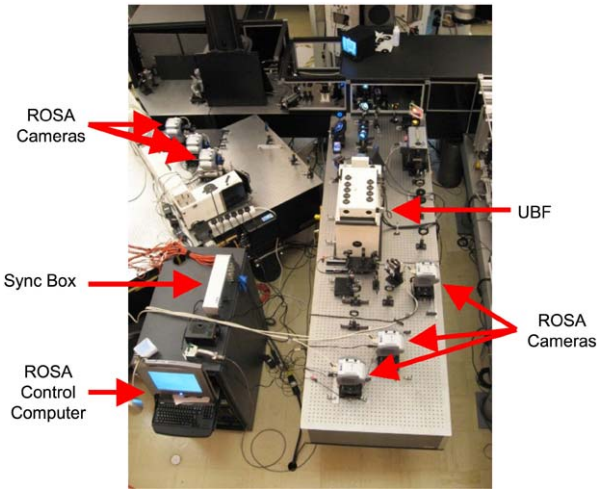

Figure 1 Six ROSA cameras placed on two optical benches at the DST during the commissioning run in August 2008. Three cameras are positioned behind "blue" filters (G-band, 4170 Å continuum and Ca-K core; left optical bench), while the remaining three cameras are positioned behind "red" filters (Hα core and circularly-polarized measurements at 6302 Å; right optical bench). One of the rack-mounted storage assemblies is also visible towards the lower-left side of the image.

keep the file size manageable, with each image written to a separate extension including only a time stamp in its header information. There are currently two available options to transfer ROSA data to external media. The first is through use of three LTO3 tape autoloaders attached to the ROSA instrument. Each tape autoloader can hold ten 400 GB uncompressed LTO3 tapes, providing the ability to back up approximately 11 TB of data. An alternative mechanism to transport data is via user-supplied external media. Hard drives equipped with a USB adaptor can connect directly to the storage computers, thus allowing for the quick transfer of data to external media and avoiding the bottleneck created when using traditional FTP or SSH commands over a network. It is anticipated that an e-SATA connection will be made available on each ROSA storage computer in the near future to further accelerate data backups.

2.1. Electron Multiplying CCDs

A solar imaging system capable of acquiring high sustained frame rates places unprecedented demands on detector technology. In particular, the short exposure times needed to maintain high-cadence imaging often leads to photon starvation, producing grainy and lacklustre solar images. However, in early 2000, Electron Multiplying Charge Coupled Devices (EMCCDs) were developed as image sensors capable of detecting single photon events without an image intensifier. This was achieved by way of a unique electron-multiplying structure built directly into the chip, and it enables solar observers to attain high-contrast images without the drawbacks associated with long exposure times (Denvir and Conroy, 2003).

A key characteristic of EMCCDs is that they are not limited by the readout noise of the chip's output amplifier like a conventional CCD, even when operated at high readout speeds. This is achieved by allowing weak signals to be multiplied before any readout noise is added through the output amplifier through the addition of a solid-state electron-multiplying register to the end of the normal serial register (Coates *et al.*, 2004). Camera readout noise is less than 15 $\mathrm{e\,s^{-1}\,pixel^{-1}}$. This measurement is for the entire system and includes a combination of CCD readout noise and analog-to-digital convertor noise. The value is for single-pixel readout with a zero-second exposure under dark conditions with unit electron-multiplication gain. The electron-multiplying register has several hundred stages that use higher than normal clock voltages, allowing for impact ionization of secondary electrons,

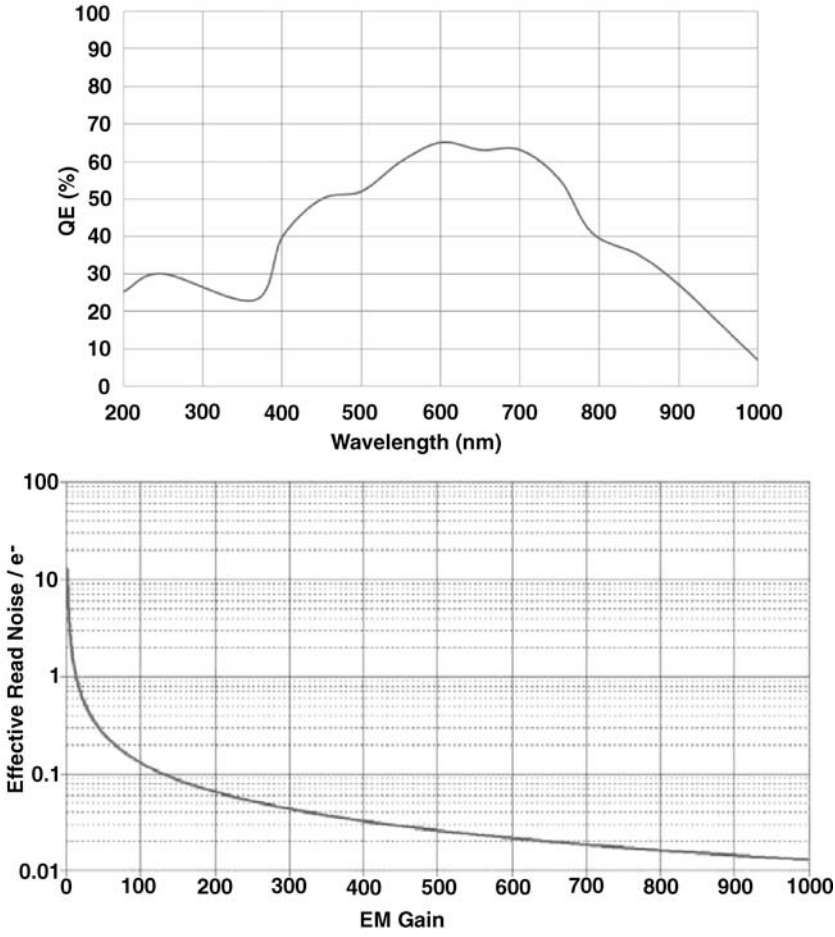

Figure 2 The upper panel is a representation of a ROSA camera's quantum efficiency as a function of wavelength, while the bottom panel plots a ROSA camera's effective read noise as a function of electron-multiplying gain. In this instance, the effective read noise is a combination of CCD readout noise and analog-to-digital convertor noise.

and hence electron gain. Through the use of hundreds of stages, the resultant gain can be user controlled to provide an amplification ranging from unity to more than several thousand. In this regime, the effective system readout noise is reduced to below 1 e s^{-1} $pixel^{-1}$, often reaching 0.02 e s^{-1} $pixel^{-1}$ under optimal conditions. Typical variations of readout noise with respect to electron multiplication are displayed in the lower panel of Figure 2.

With EMCCDs not requiring an image intensifier, quantum efficiencies as high as 95% can be obtained. The quantum efficiencies of the ROSA cameras with respect to incident wavelength is plotted in the upper panel of Figure 2. It is the combination of a minimal noise floor and a high quantum efficiency which renders the new breed of EMCCDs the most suitable for high-cadence solar imaging systems. However, it must be noted that the electron-multiplication process will inherently introduce additional noise. As a result, electron multiplication is best implemented when short exposure times and low-transmission filters result in weak incident photon counts (*i.e.* when CCD readout noise dominates). Fur-

thermore, the application of gain will reduce the number of camera applications by bringing the saturation point to lower flux levels. Care must therefore be taken when setting an electron-multiplication gain that maximizes the detection of faint features while still keeping brighter areas below their saturation point. Physically, EMCCDs resemble a conventional frame-transfer CCD structure, whereby an image is captured in the exposed region, before being shifted behind a masked storage area and being read out.

3. Observing Modes

ROSA was successfully commissioned on the 76 cm DST during August 2008 (Figure 1). It utilizes the DST's large optical benches and high-order adaptive optics to achieve multi-wavelength observations of the lower solar atmosphere. Due to the wide range of optical components available, a large number of filter combinations can be achieved. However, details of several key optical elements are outlined here.

A Zeiss universal birefringent filter (UBF; Bonaccini *et al.*, 1989) may be implemented for narrowband (≈ 0.2 Å) imaging. However, due to a significant decrease in the transmission profile of the UBF at shorter wavelengths ($\sim 0.4\%$ at 4000 Å, to be compared to $\sim 7.2\%$ at 7000 Å; Beckers, Dickson, and Joyce, 1975), it is more desirable to allow the UBF to obtain filtergrams in the "red" portion of the optical spectrum. Typically, the UBF is most commonly used for chromospheric Hα core imaging at 6562.8 Å. However, in addition to optical imaging, the UBF may be used in conjunction with a Wollaston prism to capture photospheric magnetic-field information at high spatial and temporal resolution. By tuning the UBF into the wing of the magnetically sensitive Fe I (6302.5 Å) absorption line, two ROSA cameras may be used to capture simultaneous Stokes V observations of left- and right-hand circularly-polarized light, allowing the magnitude of the line-of-sight magnetic-field component to be studied. If it is desirable to obtain magnetic-field information in the photosphere, simultaneous narrowband Hα core imaging can still be obtained using an additional tunable Zeiss filter.

For imaging in the "blue", independent Halle/Oriel filters may be used which have a more efficient transmission curve for this portion of the electromagnetic spectrum. Examples include wideband continuum and G-band filters for photospheric imaging, as well as a Calcium-K core filter for observations of the upper photosphere/lower chromosphere. Typically, observers will choose to reduce the overall field-of-view size in exchange for higher spatial resolution. In order to do this, acquired images should have a sampling of $\approx 0.07''$ per pixel to match the telescope's diffraction-limited resolution in the "blue" portion (*e.g.* 4170 Å) of the optical spectrum to that of the CCD. Doing so places 50 km of the solar surface on each pixel, providing 100 km spatial resolution and an overall field-of-view size of $50\,200 \times 50\,100$ km^2. Maintaining the same spatial sampling across all ROSA cameras will insure the resulting data to have the same field-of-view. However, users may choose to match the telescope's diffraction-limited resolution in each of their desired bandpasses to that of the CCD, thus providing optimal spatial resolution on all ROSA cameras.

Details of the most common filters may be found in Table 2. Exposure times listed are typical of quiet-Sun, disk-center observations filling approximately one-third of the well depth per exposure. Utilizing count rates obtained during the ROSA commissioning run (incorporating the default plate-scale sampling of $0.07''$ per pixel) and the camera's quantum efficiency curve (upper panel of Figure 2), photon count-rate statistics can be derived, as listed in the fifth column of Table 2. Since ROSA utilizes a host of independent computers

Table 2 Parameters related to key optical filters which may be used in conjunction with ROSA. Values which still require clarification are listed as "TBD".

Filter Name	Central Wavelength (Å)	Filter Bandpass (Å)	Typical Exp Time (ms)	Photon Count Statistics (pixel^{-1}s^{-1})	Height of Formation (km)
Ca-K core	3933.7	1.00	200	68 000	< 1300[a]
Blue continuum	4170.0	52.00	10	1 928 000	< 250
Blue continuum	3501.0	102.00	TBD	TBD	< 250
G-band	4305.5	9.20	15	1 189 000	< 250[b,c]
Magnetograms	6302.5	0.21[d]	240	80 000	< 180[e]
UBF	variable[d]	0.21[d]	variable	variable	variable
Hα core (Zeiss)	6562.8	0.25[f]	240	42 000	< 1500[g]

[a]Beebe and Johnson (1969).

[b]Uitenbroek and Tritschler (2006).

[c]Rimmele (2004).

[d]Beckers, Dickson, and Joyce (1975).

[e]Alamanni *et al.* (1990).

[f]Balasubramaniam (2002).

[g]Vernazza, Avrett, and Loeser (1981).

and storage devices, it is not necessary to run all six cameras during a single observing sequence. Indeed, any combination of cameras may be used depending on the observers' scientific requirements.

4. User Interface

A user can individually adjust camera operating temperatures, frame rates and exposure times through use of a simple graphical user interface (GUI; Figure 3). The GUI utilizes a Java-script interface to create a stable platform incorporating drop-down menus in an easy-to-follow environment. Through the GUI, users can also select which cameras to run, and modify their triggering sequence to maximize individual camera frame rates and insure the synchronization of specific cameras.

The GUI also allows the user to select which type of observations will be acquired by selecting the desired option. These options include solar data acquisition, dark images with a closed shutter, bias frames using a zero-second exposure time and flat-field images. Each choice will result in the saved filename being modified to include the desired option, thus making post-acquisition file searching much easier. Once an observing sequence has commenced, the GUI displays sample images coming from each of the cameras refreshed approximately every second. A detailed description of the GUI and a guide to its adjustable parameters may be found in the ROSA User Manual, available at http://star.pst.qub.ac.uk/rosa.

5. Calibration Data

Due to the high sensitivity of the ROSA system, it is imperative to accompany data imaging sequences with a range of additional observations. It is these supplementary observations

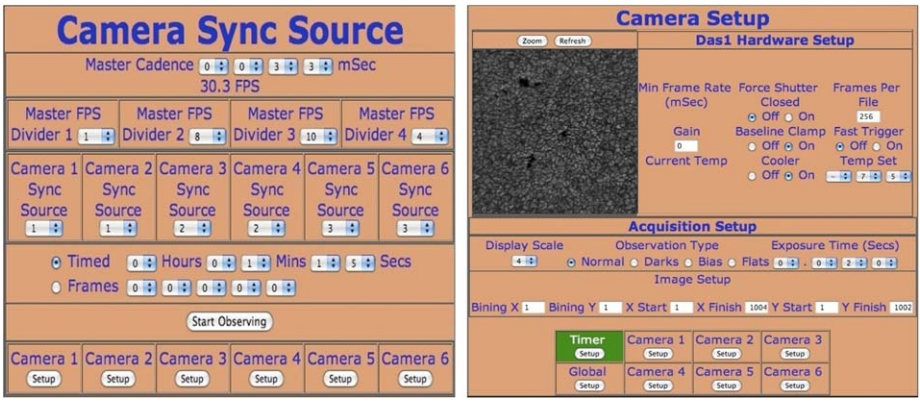

Figure 3 Screenshots of the ROSA GUI during system synchronization (left) and camera setup (right). Key input parameters can be set such as the master and secondary frame rates, which cameras are active and the desired system run time (left) in addition to the exposure time, shutter setting and camera temperature (right) before an observing sequence has commenced.

which allow accurately processed images to be produced via the ROSA-specific data reduction pipeline. To compensate for dark current and readout noise, sufficient dark images (> 250) with exposure times equal to the data acquisition must be obtained and subtracted from the science images. Many flat-field images (> 500) should also be taken through an un-flat telescope mirror coupled to a random guider to allow an accurate gain table to be created for each ROSA camera. These key calibration procedures will enable science data to be corrected for camera inconsistencies as well as for variable light levels across the incident beam. At this stage, PFIR techniques such as speckle (Weigelt and Wirnitzer, 1983) or multi-object multi-frame blind deconvolution (van Noort, Rouppe van der Voort, and Löfdahl, 2005) may be implemented. Indeed, Wöger, von der Lühe, and Reardon (2008) have shown how modern PFIR techniques can produce reconstructed images which are photometrically accurate, allowing reliable studies of solar structures to be undertaken.

However, image reconstruction processes are extremely CPU intensive and this must be taken into consideration before attempting to reduce the data. For example, during the commissioning run a single ROSA camera obtained over 105 000 raw G-band filtergrams in only one hour of observing. With excellent seeing conditions, an image reconstruction of $16 \rightarrow 1$ was deemed suitable, providing a reconstructed cadence of 0.5 s. Thus, over 6500 separate reconstructions were required, with each individual process taking approximately 30 CPU minutes to complete on a modern Intel Xeon processor. If access to only one computer is possible (*e.g.* preparing the data solely on the user's desktop PC), then reconstructing all 6500 images would take in excess of 135 days, with additional time being required to process the data from the remaining five ROSA cameras. As telescope schedules often grant individuals in excess of seven days observing time, and each day commonly provides 2 – 3 hours of good seeing conditions, it is imperative to consider how and where the acquired observations will be reduced, so excessive time delays are not experienced.

In order to co-align each ROSA camera, additional calibration images should be acquired. Images of an Air-Force target will allow compensation for general rotation and image mirroring, while acquiring a burst of grid images will enable small-scale inter-camera image rotation to be evaluated and removed. With these camera positioning artifacts removed, image destretching can be accomplished through use of the ROSA data reduction

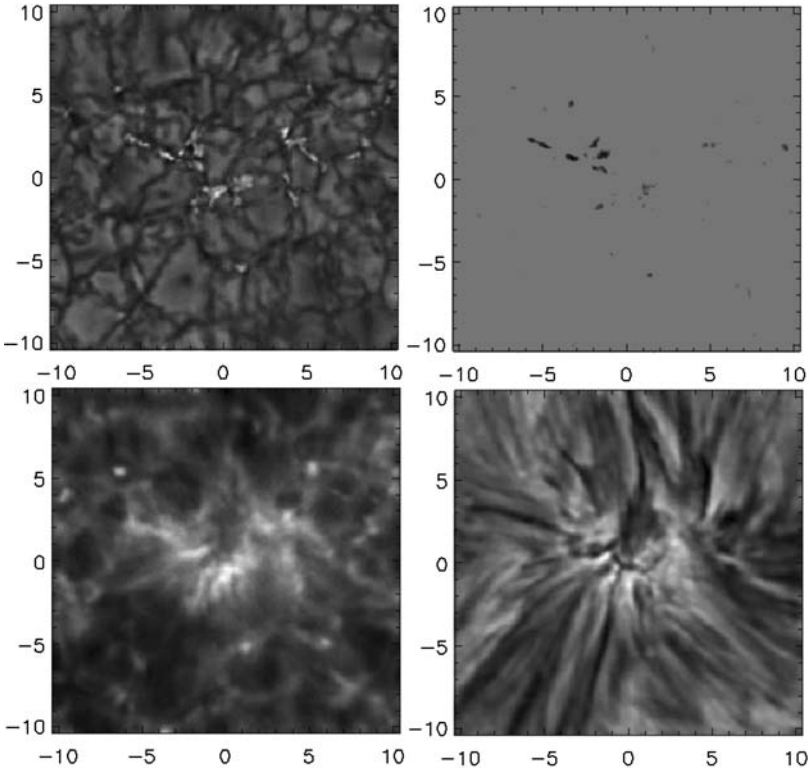

Figure 4 Simultaneous images acquired with ROSA during the commissioning run in August 2008. The top left panel shows a collection of magnetic bright points visible as intensity enhancements through the G-band filter, whereas the top right panel reveals a line-of-sight magnetogram established from difference imaging of the Stokes V parameters obtained from the magnetically sensitive Fe I absorption line at 6302.5 Å. The lower left image is a co-temporal and co-spatial representation of the upper photosphere/lower chromosphere through the Ca-K core filter and the lower right panel is how the collection of magnetic bright points look through the chromospheric Hα filter. The field-of-view (axes in arcseconds) shown here is approximately $20'' \times 20''$ or $15\,000 \times 15\,000$ km^2.

pipeline. Under normal circumstances, a 40×40 grid, equating to a $1.7''$ separation between spatial samples (for diffraction-limited resolution at 4170 Å), is used to evaluate local offsets between successive images, allowing compensation for spatial distortions caused by atmospheric turbulence and/or air bubbles crossing the entrance aperture of the telescope. The fine destretching grid implemented in this process allows for compensation for small-scale seeing conditions of $1''$ to $2''$ in size.

To help facilitate and expedite data preparation, QUB have developed a parallel processing cluster dedicated to ROSA data reduction. This cluster consists of 25 Intel Xeon quad-core CPUs providing 100 processing nodes on a dedicated private network. Users of the ROSA instrument may opt for all data reduction to be carried out on the QUB cluster, or may avail of the freely distributed ROSA pipeline for use on their own reduction cluster. The accurate reconstruction, co-alignment and destretching of multiple atmospheric heights will promote the use of multi-wavelength studies, whereby the cause of dynamic phenomena can be probed and analyzed, with the subsequent effect on other layers of the solar atmosphere evaluated.

6. Conclusions

In recent years, the solar community has expressed a strong desire for a high-cadence, synchronized, multi-camera system to be introduced which would allow for unprecedented spatial *and* temporal resolutions of solar structures over a wide range of atmospheric heights. With the successful commissioning of the ROSA instrument, it is now possible to observe solar structures at high cadences in up to six independent wavelengths simultaneously. Figure 4 shows the capabilities of observing in at least four synchronized wavelengths (G-band filtergrams, magnetograms from circularly-polarized light at 6302.3 Å, Ca-K core imaging at 3933.7 Å and narrowband Hα core filtergrams). These types of high-resolution images present an excellent opportunity to scientists, whereby magnetic structures can be investigated at multiple atmospheric heights with temporal resolutions exceeding ten frames per second.

Due to the rack-mounted nature of the ROSA instrument, future upgrades to the system can be readily carried out. As technology improves and the size of components decrease, ROSA hardware can be updated continually to keep it at the forefront of high-cadence imaging. Such upgrades will include the increased capacity of onboard storage, an improved connectivity for external media (*e.g.* e-SATA and firewire connections) and a turbulence-reducing method of camera cooling (*e.g. via* water cooling). With backside-illuminated CCDs now appearing in the marketplace, existing ROSA cameras may be replaced with such devices. In instances where low exposure times are required, this new breed of camera may lead to performance boosts in photon-starved regimes by offering a higher quantum efficiency when compared to traditional front-illuminated devices. The ability to adapt ROSA with continually changing demands and computer architecture has identified ROSA as a bridging instrument for the Advanced Technology Solar Telescope and places a high-cadence solar imager in line to become a first-light instrument on this revolutionary facility in 2015.

Acknowledgements This work was supported by the U.K. Science and Technology Facilities Council and D.B.J. wishes to thank the Science and Technology Facilities Council for the award of a Post-Doctoral Fellowship. F.P.K. is grateful to AWE Aldermaston for the award of a William Penney Fellowship. P.J.C. thanks the Northern Ireland Department for Employment and Learning for a PhD studentship. Observations were obtained at the National Solar Observatory, operated by the Association of Universities for Research in Astronomy, Inc. (AURA), under cooperative agreement with the National Science Foundation. Finally, we would like to thank the technical staff at the DST for perseverance in the face of seemingly endless camera and filter arrangements.

References

Alamanni, N., Bertello, L., Righini, A., Cavallini, F., Ceppatelli, G.: 1990, *Astron. Astrophys.* **231**, 518.
Balasubramaniam, K.S.: 2002, *Astrophys. J.* **575**, 553.
Banerjee, D., Erdélyi, R., Oliver, R., O'Shea, E.: 2007, *Solar Phys.* **246**, 3.
Beckers, J.M., Dickson, L., Joyce, R.S.: 1975, *A Fully Tunable Lyot-Öhman Filter*, AFCRL-TR-75-0090; Bedford: AFCRL.
Beebe, H.A., Johnson, H.R.: 1969, *Solar Phys.* **10**, 79.
Bonaccini, D., Righini, A., Cavallini, F., Ceppatelli, G.: 1989, *Astron. Astrophys.* **217**, 368.
Brown, J.C.: 1971, *Solar Phys.* **18**, 489.
Coates, C.G., Denvir, D.J., McHale, N.G., Thornbury, K.D., Hollywood, M.A.: 2004, *J. Biomed. Opt.* **9**, 1244.
Denvir, D.J., Conroy, E.: 2003, *Proc. SPIE* **4877**, 55.
Deubner, F.-L.: 1975, *Astron. Astrophys.* **44**, 371.
Hanisch, R.J., Farris, A., Greisen, E.W., Pence, W.D., Schlesinger, B.M., Teuben, P.J., Thompson, R.W., Warnock, A.: 2001, *Astron. Astrophys.* **376**, 359.

Hasan, S.S., van Ballegooijen, A.A.: 2008, *Astrophys. J.* **680**, 1542.
Jess, D.B., Andić, A., Mathioudakis, M., Bloomfield, D.S., Keenan, F.P.: 2007a, *Astron. Astrophys.* **473**, 943.
Jess, D.B., McAteer, R.T.J., Mathioudakis, M., Keenan, F.P., Andic, A., Bloomfield, D.S.: 2007b, *Astron. Astrophys.* **476**, 971.
Katsiyannis, A.C., Williams, D.R., McAteer, R.T.J., Gallagher, P.T., Keenan, F.P., Murtagh, F.: 2003, *Astron. Astrophys.* **406**, 709.
Kiplinger, A.L., Dennis, B.R., Frost, K.J., Orwig, L.E., Emslie, A.G.: 1983, *Astrophys. J.* **265**, L99.
Leighton, R.B.: 1960, *Proc. IAU Symp.* **12**, 321.
Phillips, K.J.H., Read, P.D., Gallagher, P.T., Keenan, F.P., Rudawy, P., Rompolt, B., Berlicki, A., Buczylko, A., Diego, F., Barnsley, R., Smartt, R.N., Pasachoff, J.M., Babcock, B.A.: 2000, *Solar Phys.* **193**, 259.
Porter, L.J., Klimchuk, J.A., Sturrock, P.A.: 1994, *Astrophys. J.* **435**, 502.
Rimmele, T.R.: 2004, *Astrophys. J.* **604**, 906.
Uitenbroek, H., Tritschler, A.: 2006, *Astrophys. J.* **639**, 525.
van Noort, M., Rouppe van der Voort, L., Löfdahl, M.G.: 2005, *Solar Phys.* **228**, 191.
van Noort, M.J., Rouppe van der Voort, L.H.M.: 2006, *Astrophys. J.* **648**, L67.
Vernazza, J.E., Avrett, E.H., Loeser, R.: 1981, *Astrophys. J. Suppl.* **45**, 635.
Wang, H., Qiu, J., Denker, C., Spirock, T., Chen, H., Goode, P.R.: 2000, *Astrophys. J.* **542**, 1080.
Weigelt, G., Wirnitzer, B.: 1983, *Opt. Lett.* **8**(7), 389.
Williams, D.R., Phillips, K.J.H., Rudawy, P., Mathioudakis, M., Gallagher, P.T., O'Shea, E., Keenan, F.P., Read, P., Rompolt, B.: 2001, *Mon. Not. Roy. Astron. Soc.* **326**, 428.
Williams, D.R., Mathioudakis, M., Gallagher, P.T., Phillips, K.J.H., McAteer, R.T.J., Keenan, F.P., Rudawy, P., Katsiyannis, A.C.: 2002, *Mon. Not. Roy. Astron. Soc.* **336**, 747.
Wöger, F., von der Lühe, O., Reardon, K.: 2008, *Astron. Astrophys.* **488**, 375.